GEOPHYSICS, VOL. 86, NO. 1 (JANUARY-FEBRUARY 2021); P. Q1–Q13, 17 FIGS., 1 TABLE.
10.1190/GEO2019-0208.1

Check for updates

Downloaded 05/13/21 to 145.94.67.71. Redistribution subject to SEG license or copyright; see Terms of Use at http://library.seg.org/page/policies/terms
DOI:10.1190/geo2019-0208.1

Interferometric redatuming by deconvolution and correlation-based focusing

Diego F. Barrera[1], Joerg Schleicher[2], and Joeri Brackenhoff[3]

ABSTRACT

Seismic interferometry is a method used to calculate wavefields for sources and receivers that are located where only sources or only receivers are available. There are correlation- or deconvolution-based interferometric methods that can be used to reposition the seismic array from the earth's surface to an arbitrary datum at depth. Based on the one-way reciprocity theorems of convolution and correlation type, we have determined that interferometric redatuming can be achieved in a deconvolution-only procedure in three steps. The first two steps consist of separately retrieving, for sources at the earth's surface, the downward- and upward-propagating Green's functions at receivers at the datum, which are then used in the third step to reposition the sources to the datum. For the involved deconvolutions, transmitted and backscattered wavefields need to be modeled with a velocity model between the acquisition and datum levels. Our numerical experiments demonstrate that the method can help to reduce nonphysical events and other artifacts that commonly arise in purely correlation-based procedures. If a high-quality overburden-velocity model is available, it correctly accounts for inhomogeneities in the overburden medium. Because the method's sensitivity to the velocity model is mainly introduced by backscattering at overburden heterogeneities, a smooth model is sufficient when overburden scattering is weak.

INTRODUCTION

Seismic interferometry is a technique that allows for the retrieval of the Green's functions for sources at positions at which only receivers are available (or vice versa). The classic redatuming procedure correlates surface seismic data with those acquired at depth. These so-called correlation-based methods have been well-studied in the literature (see, e.g., Wapenaar et al., 2008, 2010b; Curtis, 2009; Schuster, 2009; Curtis and Halliday, 2010; van der Neut, 2012). However, they can suffer from crosstalk between unrelated events leading to the generation of nonphysical events if the medium between the earth's surface and the datum is heterogeneous (Barrera et al., 2017).

According to Wapenaar et al. (2011), seismic interferometry by deconvolution can be an advantageous alternative to the classic correlation-based procedure because the former techniques tend to suffer less from crosstalk, in this way generating fewer acausal and other nonphysical events than the latter. The cited authors demonstrate that multidimensional deconvolution of the separated up- and downgoing wavefields for sources at the surface and receivers at depth can be used to recover the complete reflected wavefield at the datum with significantly fewer artifacts.

However, before the work of van der Neut et al. (2015a), the required wavefield constituents would be available only if actual physical receivers had been placed at depth. Still, Wapenaar et al. (2011) point out that there are many situations in which the deconvolutional form is more convenient than the correlation-based methods. One of the main advantages of the deconvolution-based procedure is its inherent compensation for the properties of the source wavelet. Another important advantage is that deconvolution-based techniques can treat internal multiples and are generally more easily extendable to lossy media (Slob and Wapenaar, 2007).

The complete deconvolutional redatuming procedure becomes feasible when van der Neut et al. (2015a) demonstrate that the required wavefield constituents for the deconvolutional procedure of Wapenaar et al. (2011) can be recovered by inverting two expressions based on the one-way reciprocity theorems with iterative Marchenko procedures.

In this work, we propose a different procedure to recover those constituents. Based on the interferometric expressions of van der

Manuscript received by the Editor 15 April 2019; revised manuscript received 11 August 2020; published ahead of production 25 October 2020; published online 27 January 2021.
[1]SENAI-CIMATEC Supercomputing Center for Industrial Innovation & INCT-GP, Av. Orlando Gomes, 1845, 41770-395 Salvador, Bahia, Brazil. E-mail: diegofernando84@gmail.com (corresponding author).
[2]IMECC/UNICAMP & INCT-GP, Rua Sergio Buarque de Holanda, 651, 13083-859 Campinas, SP, Brazil. E-mail: js@ime.unicamp.br.
[3]Delft University of Technology, Department of Geotechnology, Mijnbouwstraat 120, 2628 RX Delft, The Netherlands. E-mail: j.a.brackenhoff@tudelft.nl.
© 2021 Society of Exploration Geophysicists. All rights reserved.

Downloaded 05/13/21 to 145.94.67.71. Redistribution subject to SEG license or copyright; see Terms of Use at http://library.seg.org/page/policies/terms
DOI:10.1190/geo2019-0208.1

Neut et al. (2015a), we combine deconvolution-based interferometry with inverse wavefield extrapolation to derive an alternative procedure for retrieving the total wavefield at the datum. Inverse wavefield extrapolation is a concept used to describe the process of retrieving the Green's functions at an arbitrary datum by means of backpropagation of the wavefield recorded at the earth's surface (van der Neut et al., 2015b; van der Neut and Wapenaar, 2016). Our proposed procedure consists of a deconvolution process that is carried out as a convolution with the adjoint (modeled) wavefield, followed by a convolution with the inverse point-spread function (PSF), i.e., the autocorrelation of the modeled wavefield. We apply this deconvolution process to the equations of van der Neut et al. (2015a) to determine the downward- and upward propagating Green's functions at the datum for a point source at the earth's surface. These down- and upgoing Green's functions are then used in a third deconvolution step to retrieve the primary-reflected wavefield at the datum.

Using this new approach, we set up a fully deconvolutional procedure that reduces the influence of the overburden, which can manifest itself in the redatumed data in the form of multiples, spurious events of the Green's functions, and anticausal events. The information required for the proposed technique is a velocity model of the overburden medium. This model is used to simulate the (vertical derivative of the) transmitted wavefield from the surface source to the datum as well as the overburden-scattered wavefield at the surface and its vertical derivative. If sufficient detail in the overburden model is available, the proposed procedure will correctly treat the effects of overburden inhomogeneities.

THEORY

In this section, we derive the theory of the proposed deconvolution-based interferometric redatuming procedure. For this purpose, we revisit the derivation of the reciprocity theorems using the Helmholtz equation with velocity and density variation. These derivations are fundamental to understand the wavefield expressions in different cases. The basic form, using a closed surface, is the ideal case for the reciprocity theorems, but special conditions make it possible to consider less ideal situations. In particular, we focus on the one-way reciprocity theorems of the correlation and convolution type. These theorems represent the platform upon which we derive the relationships allowing for up- and downward inverse wavefield propagation.

Basic equations

In this work, the Fourier-transform pair relating a time-dependent function $d(t)$ to its frequency spectrum $\hat{d}(\omega)$ is defined as

$$\hat{d}(\omega) = \int_{-\infty}^{\infty} d(t)\exp(i\omega t)dt, \tag{1}$$

$$d(t) = \frac{1}{2\pi}\int_{-\infty}^{\infty} \hat{d}(\omega)\exp(-i\omega t)d\omega, \tag{2}$$

where i is the imaginary unit and ω denotes the angular frequency. The integration domain in equation 1 can be decomposed in two time intervals, $(-\infty, 0]$ and $[0, \infty)$. According to Bleistein et al. (2001), the time dependence of some wavefield associated with a source starts at $t = 0$. Then, the second interval above corresponds to the causal part of function $d(t)$, whereas the first interval corresponds to its anticausal part, i.e., the wavefield described at some time in the past and imploding toward a source at time zero.

Temporal Fourier transformation of the acoustic wave equation with variable density leads to the corresponding Helmholtz equation, which can be written as (Bleistein et al., 2001)

$$\rho(x)\nabla\cdot\left[\frac{1}{\rho(x)}\nabla\hat{p}(x,\omega)\right] + \frac{\omega^2}{c^2(x)}\hat{p}(x,\omega) = -\hat{F}(x,\omega). \tag{3}$$

Here, $x = (x_1, x_2, x_3)$ with the subscripts numbering the coordinate axes. Operator ∇ is defined as the gradient and represents the derivatives with respect to the spatial coordinates. Moreover, $\rho(x)$ denotes the variable density, $\hat{p}(x,\omega)$ denotes the pressure field, $c(x)$ is the spatially varying wave velocity, and $\hat{F}(x,\omega)$ is a source term. In the particular case of a temporal and spatial point source at position x^s and time $t = 0$ s, the source term is given by a delta function $\delta(x - x^s)$. Then, the pressure field is represented by the Green's function $\hat{G}(x,\omega;x^s)$, which must satisfy

$$\rho(x)\nabla\cdot\left[\frac{1}{\rho(x)}\nabla\hat{G}(x,\omega;x^s)\right] + \frac{\omega^2}{c^2(x)}\hat{G}(x,\omega;x^s) = -\delta(x-x^s). \tag{4}$$

The basis for seismic interferometry is Gauss's divergence theorem, which relates an integral over a closed surface ∂V of an arbitrary vector field $\rightarrow \Psi$ to an integral over the enclosed volume V of the divergence of the vector field, i.e.,

$$\oiint_{\partial V} \overrightarrow{\Psi}\cdot\hat{n}dS = \iiint_V \nabla\cdot\overrightarrow{\Psi}dV, \tag{5}$$

where $\hat{n}$ is the unit vector normal to surface ∂V pointing in the outward direction of volume V. Equation 5 is the basis for the derivation of the one-way reciprocity theorems of convolution and correlation type in Appendix A.

Up- and downgoing Green's functions

Using the one-way reciprocity theorems of convolution and correlation type, equations A-16 and A-19, it is possible to retrieve the upward- and downward-propagating wavefields at an arbitrary datum in depth. For this purpose, we still need to specify these expressions to the specific situation under consideration. Note that the resulting relationships are previously derived by van der Neut et al. (2015a) in the context of Marchenko imaging. Here, we give them a new interpretation and use them for a deconvolution-based interferometric redatuming technique.

To derive these relationships in our notation, we start again at two states, A and B (indicated by superscripts A and B) in the frequency-space domain (Figure 1). In state A, we consider a point source positioned immediately above surface S_1. In this situation, the vertical derivative of the downgoing wavefield at the surface can be expressed as $\partial_3\hat{p}_+^A = (-1/2)\delta(x - x^A)$ (Wapenaar et al., 2014). The validity region of this expression in state A is limited by surfaces S_1 and S_2. Between these surfaces, the medium may be arbitrarily inhomogeneous. Above S_1 and below S_2, we consider homogeneous half-spaces without a free surface (Figure 1). We will refer to the velocity model in state A as the truncated model.

Downloaded 05/13/21 to 145.94.67.71. Redistribution subject to SEG license or copyright; see Terms of Use at http://library.seg.org/page/policies/terms
DOI:10.1190/geo2019-0208.1

In state B, we consider the same inhomogeneous medium between surfaces S_1 and S_2 as in state A. Above S_1, we still consider a homogeneous medium half-space without a free surface, and below S_2 we now consider a scattering body. The source in state B is also a point source immediately above surface S_1, such that the vertical derivative of the downgoing wavefield can be represented as $\partial_3 \hat{p}^B_+ = (-1/2)\delta(x - x^B)$ (Wapenaar et al., 2014).

In states A and B, we consider the wavefield decomposition into up- and downgoing constituents in analogy to equation A-11. An analysis of the physical situation in both states allows for an interpretation of all propagating events at every surface in Figure 1, resulting in Table 1.

Substitution of the wavefield expressions from Table 1 in the one-way reciprocity theorem of convolution type, equation A-16, leads to

$$\frac{1}{2\rho(x^A)}\hat{G}^B_-(x^A,\omega;x^B) - \frac{1}{2\rho(x^B)}\hat{G}^A_-(x^B,\omega;x^A) \approx -\iint_{S_2}\frac{1}{\rho(x')}\hat{G}^B_-(x',\omega;x^B)\partial_3\hat{G}^A_+(x',\omega;x^A)d^2x', \quad (6)$$

where we have carried out the integrations over the delta functions describing the vertical derivatives of the point-source wavefields on the left side.

Equation 6 is the first of the desired relationships, allowing us to arrive at the first step of our main theoretical result, which is the following observation: this expression allows us to invert for the upgoing Green's function $\hat{G}^B_-(x',\omega;x^B)$ at the datum S_2 if we know the corresponding Green's function $\hat{G}^B_-(x^A,\omega;x^B)$ at the surface S_1 (i.e., the surface data). All we need for that purpose is the knowledge of the overburden velocity field between S_1 and S_2, so that we can model, for a source at x_A, the backscattered Green's function $(1/(\rho(x^B)))\hat{G}^A_-(x^B,\omega;x^A)$ at x_B as well as the derivatives of the transmitted Green's function $(1/(\rho(x')))\partial_3\hat{G}^A_+(x',\omega;x^A)$ for all points x' on surface S_2 (see Figure 1).

In the full analogy, we can replace the wavefield expressions of Table 1 in the one-way reciprocity theorem of the correlation type (equation A-19) to obtain the second important relationship,

$$\frac{1}{2\rho(x^B)}\hat{G}^{A*}_+(x^B,\omega;x^A) + \iint_{S_1}\frac{1}{\rho(x)}\hat{G}^B_-(x,\omega;x^B)\partial_3\hat{G}^{A*}_-(x,\omega;x^A)d^2x \approx -\iint_{S_2}\frac{1}{\rho(x')}\hat{G}^{A*}_+(x',\omega;x^A)\partial_3\hat{G}^B_+(x',\omega;x^B)d^2x', \quad (7)$$

which allows us to invert for the vertical derivative of the downgoing Green's function $\partial_3\hat{G}^B_+(x',\omega;x^B)$ at the datum using the surface data $\hat{G}^B_-(x,\omega;x^B)$. For this purpose, we again need only the overburden velocity model to be able to simulate three wavefields associated with state A for a point source at x^A. These are (1) the complex conjugate of the transmitted wavefield $\hat{G}^{A*}_+(x',\omega;x^A)$ from the earth's surface (S_1) to the datum (S_2), (2) its density-normalized vertical derivative $(1/(\rho(x')))\partial_3\hat{G}^{A*}_+(x',\omega;x^A)$, and (3) the complex conjugate of the backscattered wavefield $(1/(\rho(x)))\hat{G}^{A*}_-(x,\omega;x^A)$ at the surface S_1.

Note that van der Neut et al. (2015a) propose to invert equations 6 and 7 by means of an iterative Marchenko scheme to determine the inverse operators to G^A_+ and its complex conjugate. In this work, we invert these equations by means of a damped least-squares deconvolution, so as to derive an interferometric redatuming in which all steps are deconvolution-based.

Deconvolution-based interferometric redatuming

Our new interpretation of the above equations is fundamental because it shows that they allow for retrieving the down- and upgoing constituents of the Green's functions for sources at the surface and receivers at the datum by means of deconvolution. These wavefields are, in turn, the ingredients for redatuming the sources using the classic expression for deconvolution-based interferometric redatuming of Wapenaar et al. (2011). This expression is set up by noting that each trace $\hat{G}^B_-(x'',\omega;x^B)$ in the output gather can be interpreted as the stack of a convolution gather, which is obtained by convolution of each trace in the reflection response $\hat{R}(x'',\omega;x')$ at the datum for a fixed source point x'' with each trace of the vertical derivative $\partial_3\hat{G}^B_+(x',\omega;x^B)$ of the downgoing wavefield constituent for a fixed source position x^B at the surface and all receiver positions x' at the datum. Thus, mathematically, the deconvolution-based redatuming equation can be expressed in the case of variable density as

$$\hat{G}^B_-(x'',\omega,x^B) = -2\rho(x'') \times \iint_{S_2}\int\frac{1}{\rho(x')}\hat{R}(x'',\omega;x')\partial_3\hat{G}^B_+(x',\omega;x^B)d^2x'. \quad (8)$$

The main objective of this work is to introduce equations 6 and 7 as tools to determine, by means of deconvolution, the input to equation 8, i.e., the up- and downward Green's function constituents $(1/(\rho(x'')))\hat{G}^B_-(x'',\omega,x^B)$ and $(1/(\rho(x')))\partial_3\hat{G}^B_+(x',\omega;x^B)$, re-

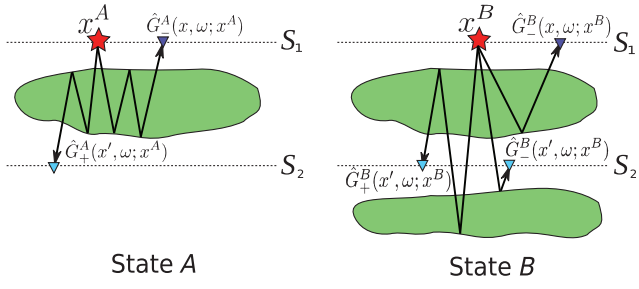

Figure 1. Two wavefield states in an inhomogeneous overburden. State A uses a truncated model to describe the transmitted wavefield from the surface and its responses recorded at the datum and at the surface. State B uses the actual velocity distribution in the subsurface to describe the total wavefield taking into account all events propagating in the medium.

Table 1. Analysis of the up- and downgoing wavefields at surfaces S_1 and S_2 in states A and B, respectively.

Surface	Direction	Wavefield in state A	Wavefield in state B
S_1	+	Point source in x^A	Point source in x^B
S_1	−	$\hat{G}^A_-(x,\omega;x^A)$	$\hat{G}^B_-(x,\omega;x^B)$
S_2	+	$\hat{G}^A_+(x',\omega;x^A)$	$\hat{G}^B_+(x',\omega;x^B)$
S_2	−	0	$\hat{G}^B_-(x',\omega;x^B)$

Downloaded 05/13/21 to 145.94.67.71. Redistribution subject to SEG license or copyright; see Terms of Use at http://library.seg.org/page/policies/terms
DOI:10.1190/geo2019-0208.1

spectively. Once these wavefield constituents are known, it is possible to retrieve the total reflected wavefield $\hat{R}(x'', \omega; x')$ at the datum using any inversion method (in this work, we use a stabilized least-squares inversion). Figure 2 explains this linear inversion problem graphically.

According to Wapenaar et al. (2011), in most situations, it is more convenient to carry out interferometry by deconvolution-based than by correlation-based expressions because the deconvolution-based procedure automatically includes a compensation for the properties of the source wavelet. Another advantage is that it does not need the assumption of a lossless medium. If the overburden velocity model is sufficiently accurate, it also provides a correct treatment of internal multiples.

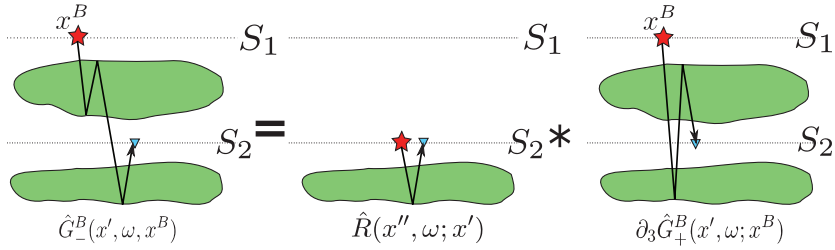

Figure 2. Sketch explaining the linear inversion problem 7. Once the one-way Green's function responses $(1/\rho(x'))\hat{G}^B_-(x'', \omega, x^B)$ and $(1/\rho(x))\partial_3 \hat{G}^B_+(x', \omega; x^B)$ at the datum have been determined in the previous steps, the reflected wavefield at the datum can be calculated by deconvolution.

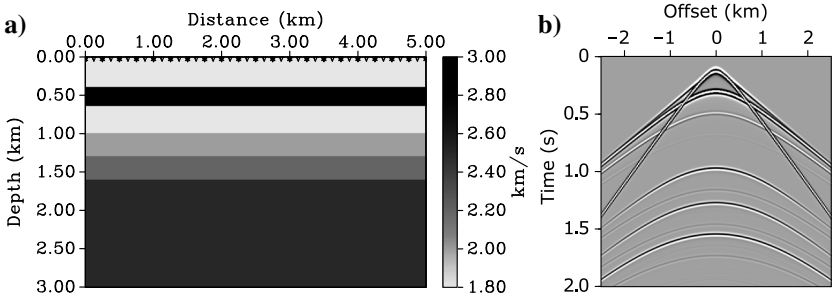

Figure 3. (a) Flat layer model with sources and receivers at the earth's surface and (b) the central shot in model (a).

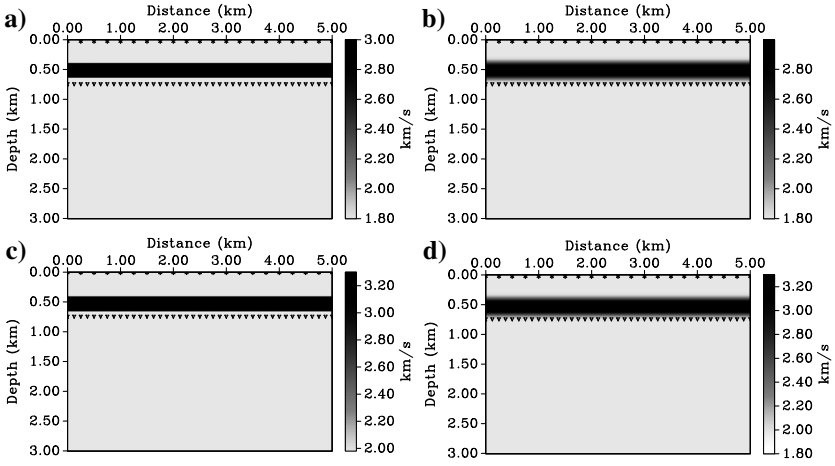

Figure 4. Overburden models that correspond to different tests for retrieving the backscattered and transmitted wavefields. The overburden velocity fields correspond to (a) the true model, (b) its smoothed version, (c) an incorrect model, and (d) its smoothed version. For details, see the text.

NUMERICAL EXPERIMENTS

To evaluate the potential of our proposed procedure of redatuming by recovering the separate wavefield constituents by means of deconvolution, we have carried out a few numerical experiments. To allow for an easier interpretation of the wavefield components in the individual steps and to discuss the results, we use synthetic data from the horizontally layered velocity model depicted in Figure 3a with layer velocities varying between 1.8 km/s and 3.0 km/s. The original acquisition geometry makes use of 201 sources spaced at 25 m and the same number of receivers for each shot, all positioned in the interval between 0.0 km and 5.0 km along the earth's surface. Figure 3b shows the shot section for the central source in the model.

Our purpose is to redatum these data to the same acquisition geometry as at the surface, but at the datum at 750 m depth. For this purpose, we need a truncated velocity model (i.e., homogeneous below the datum) to simulate (1) the transmitted wavefield from the earth's surface until the datum, (2) its corresponding vertical derivative, (3) the backscattered wavefield at the earth's surface, and (4) its corresponding vertical derivative. Using these wavefields, modeled with a velocity model of the datum overburden, we determine the down- and upward wavefield constituents for receivers at depth using equations 6 and 7, and then the redatumed wavefield with sources and receivers at the datum using equation 8.

To test the sensibility of our redatuming methodology, we use four different overburden models as the truncated velocity model. These models, depicted in Figure 4, are (1) the exact model (Figure 4a), (2) a smoothed version of the exact model (Figure 4b), obtained by passing a 15×15 sample moving-average filter over the true model, (3) an incorrect model with a mispositioned high-velocity layer and 10% too-high velocities (Figure 4c), and (4) a smoothed version of the incorrect model, obtained by passing the same moving average filter over the incorrect model (Figure 4d).

For comparison with the redatumed wavefield constituents, we simulate the full wavefield in the model of Figure 3 for one shot at the earth's surface at 2.5 km on the horizontal axis with receivers at the datum at 750 m depth (Figure 5a). The visible events in the seismic section of Figure 5a are labeled with numbers to identify them. The green arrows and numbers from 1 to 10 identify downgoing events, and the red arrows and numbers from 11 to 16 identify upgoing events. Figures 5b and 5c show the geometric interpre-

Downloaded 05/13/21 to 145.94.67.71. Redistribution subject to SEG license or copyright; see Terms of Use at http://library.seg.org/page/policies/terms
DOI:10.1190/geo2019-0208.1

tation of the labeled events by means of their raypaths. This will help us to compare the respective events with the inverted up- and downgoing wavefield constituents shown in the next sections.

Downward wavefield constituent by focusing

The first step of our proposed redatuming procedure consists of retrieving, by means of inverting equation 7, the vertical derivative of the downgoing constituents of the Green's function $\partial_3 \hat{G}_+^B(x', \omega; x^B)$ at the datum at 750 m depth.

For this inversion, we model the following input data in the truncated velocity model: (1) the vertical derivative of the transmitted wavefield from the earth's surface to a datum at 750 m depth ($\hat{G}_+^{A*}$) and (2) the vertical derivative of the backscattered wavefield with sources and receivers at the earth's surface ($\partial_3 \hat{G}_-^{A*}$).

The deconvolution procedure consists of convolving the left side of equation 7 with the transmitted wavefield $\hat{G}_+^A(x', \omega; x^A)$ at the datum and then with the inverse of the resulting PSF, which corresponds to the autocorrelation of $\hat{G}_+^A(x', \omega; x^A)$. To calculate the inverse PSF, we use a damped least-squares scheme with regularization of 0.1% of the maximum value of the PSF.

In the numerical procedure, the Green's functions $\hat{G}_+^{A*}$ and $\hat{G}_-^{A*}$ in equation 7 are replaced by wavefields $\hat{U}_+^{A*}$ and $\hat{U}_-^{A*}$ containing a source wavelet. In our synthetic examples, we use the same source wavelet for the wavefield modeling in the truncated model as for the modeling of the simulated data. Theoretically, this should not matter because the power spectrum of the source wavelet, which appears on the left side of equation 7 after convolution with $\hat{U}_+^A(x', \omega; x^A)$, is canceled by the convolution with the inverse PSF. In this way, the original source wavelet of the input data is preserved. In practice, of course, some frequency limitations apply to the inversion of the PSF, which may lead to distortions of the wavelet in the redatumed data.

Using the four overburden models of Figure 4, we numerically simulate the transmitted wavefield from the surface to the datum stations and the backscattered wavefield in the truncated medium at the surface stations and use them for deconvolution according to equations 6 and 7. Figure 6 shows the corresponding deconvolution results.

Figure 6a depicts the wavefield retrieved by means of equation 7 when modeling the transmitted and backscattered wavefields in the exact truncated velocity field. As predicted by theory, we retrieve the vertical derivative of the downward Green's function constituents. All interpretable events match the measured kinematics in the modeled data of Figure 5a. As a precursor to the first event in Figure 6a, it is possible to observe weak boundary effects related to the finite aperture in the seismic array.

When using an incorrect velocity model, the kinematics change and the relative amplitudes are no longer correct in the recovered wavefield (Figure 6b). Events 3 and 10 are even no longer visible. Moreover, the boundary effects are stronger than in Figure 6a, and some numerical artifacts appear. Overall, we observe that a relatively small velocity error already visibly affects the quality of the results.

Figure 6c and 6d shows the results when the modeling is performed using the smoothed velocity fields. We observe that, in both cases, only event 1 has been retrieved. The reason is that the smoothed models used in these cases for the wavefield modeling allow us to model first arrivals only. Therefore, the deconvolution procedure is not able to recover multiple reflections. However, the

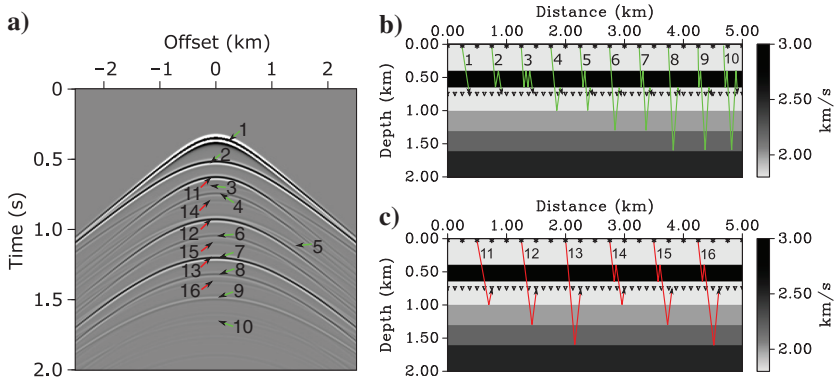

Figure 5. (a) Full synthetic seismic wavefield at the datum at 750 m depth. Labeled are the down- (the green arrows) and upgoing (the red arrows) constituents, the raypaths of which are shown in (b) and (c), respectively.

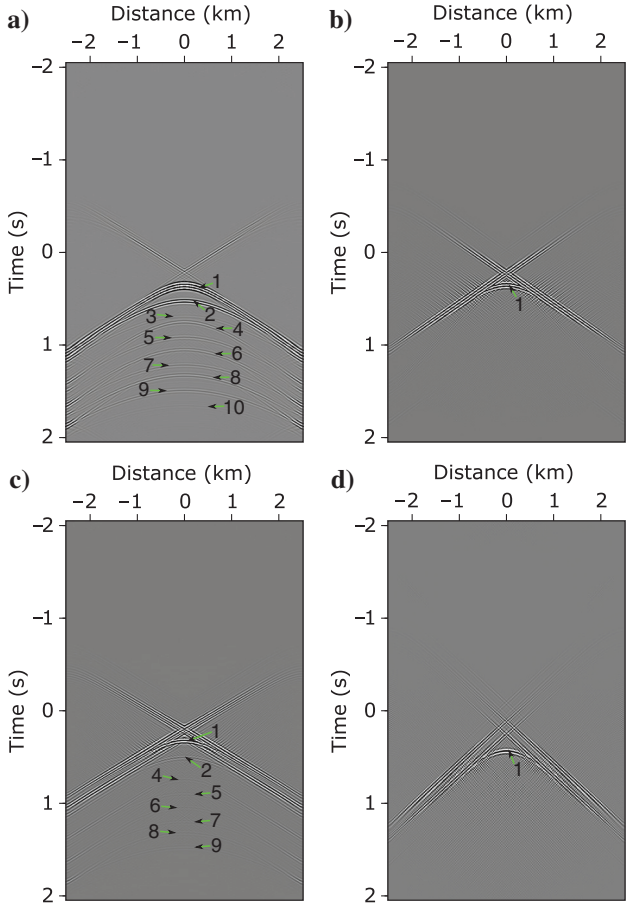

Figure 6. Downward Green's function retrieved by inversion using equation 7, using different models for wavefield modeling: (a) exact, (b) incorrect, (c) smoothed exact, and (d) smoothed incorrect model.

Downloaded 05/13/21 to 145.94.67.71. Redistribution subject to SEG license or copyright; see Terms of Use at http://library.seg.org/page/policies/terms
DOI:10.1190/geo2019-0208.1

recovered event 1 is actually better positioned when using the smoothed incorrect model (Figure 6d) than the nonsmoothed version (Figure 6b).

The situation is different in Figure 7. Here, we model the transmitted wavefield in the smoothed truncated velocity field (Figure 4b) and the backscattered wavefield in the exact version (Figure 4a). We did this because, during sensitivity tests of the method, we noted that this combination of input data allows us to retrieve most of the downward wavefield signals. However, note that events 2 and 3 are not retrieved in this response because these events are due to internal reverberations of the transmitted wavefield in the overburden. In contrast, the internal multiples from below the datum (events 4–10) are correctly recovered. Moreover, Figure 7 shows a strongly perturbed event 1 and an additional event *D*.

These effects can be interpreted as artifacts corresponding to overburden reverberations. They are generated by the deconvolution through nonphysical combination of primaries and multiples in such a way that some parts of their raypaths contribute with positive and others with negative traveltimes (see the raypaths for events *B*, *C*, and *D* in Figure 8). Note that events *B* and *C* are not easily interpretable in Figures 6 and 7 because they interfere with event 1. This experiment indicates that, if we were able to determine and separate the backscattering from overburden inhomogeneities in the input reflection seismic data, it might be possible to obtain redatuming results of the quality of Figure 7 using a smooth velocity field for the modeling of the transmitted wavefield only.

Upward wavefield constituent by focusing

In the next step, we need to determine the upward Green's function $\hat{G}^B_-(x', \omega; x^B)$ by inverting equation 6. For this purpose, we require the following input data: (1) the vertical derivative of the transmitted wavefield from the earth's surface to the datum at 750 m depth ($\partial_3 \hat{G}^A_+$) and (2) the backscattered wavefield with sources and receivers at the earth's surface ($\hat{G}^A_-$), both modeled in the truncated velocity field. As previously, we correct the deconvolution results for the PSF, in this case given by the autocorrelation of the vertical derivative of the transmitted wavefield $\partial_3 \hat{G}^A_+(x', \omega; x^A)$. Again, to retrieve the inverse PSF, we use a damped least-squares scheme with 0.1% of the maximum PSF value.

Our tests use the same four model combinations as previously to model the required synthetic data. The resulting Green's function constituents are depicted in Figure 9. We observe that, as expected, when the modeling is performed using the exact truncated model (Figure 9a), all upgoing Green's function constituents but no downgoing constituents are retrieved (compare to Figure 5a). This can be confirmed by comparing the traveltimes of the upgoing events in Figure 5c with those in Figure 9a.

When the modeling is done in the incorrect or the smoothed velocity fields (see Figure 9b–9d), all upgoing Green's function constituents are also retrieved, but three artifacts labeled A, B, and C are introduced. These events correspond to nonphysical propagation paths with negative and positive times (Figure 8). These artifacts are generated by the lack of reverberations in the wavefields calculated using the smoothed and incorrect overburden velocity fields. Figure 9b–9d looks very similar to each other. Closer inspection reveals some kinematic errors in Figure 9c and 9d because of the error in the underlying velocity models.

When modeling the transmitted wavefield in the smoothed velocity field and the backscattered wavefield in the exact velocity field, the upgoing Green's function constituents are recovered without artifacts (see Figure 10). We note that the response in Figure 10 is very similar to that in Figure 9a. Again, all events correspond to upgoing wavefield constituents. This makes us conclude that the model of the inversion using equation 6 is more sensitive to the backscattered wavefield rather than the transmitted one.

Source redatuming

The above two steps describe the redatuming of receivers so as to determine the up- and downgoing Green's function constituents for sources at the acquisition surface and receivers at the datum. To complete the redatuming process, we still need to relocate the sources to the datum level by means of inverting equation 8 for $\hat{R}(x', \omega; x'')$.

The input data for the inversion of equation 8 are the up- and downgoing Green's function constituents retrieved in the previous two steps. In accordance with our four model choices to determine these wavefields, Figure 11 shows four results of the complete redatuming procedure. For easier interpretation, we have labeled each physical event with an *R* and a number, and each nonphysical event with an *R* and a capital letter.

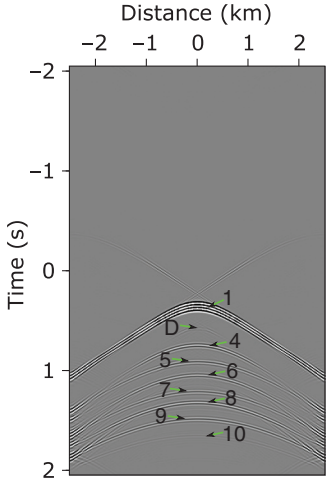

Figure 7. Downward Green's function retrieved by inversion using equation 7, using the smoothed model for the transmitted wavefield, but using the exact model for the backscattered wavefield.

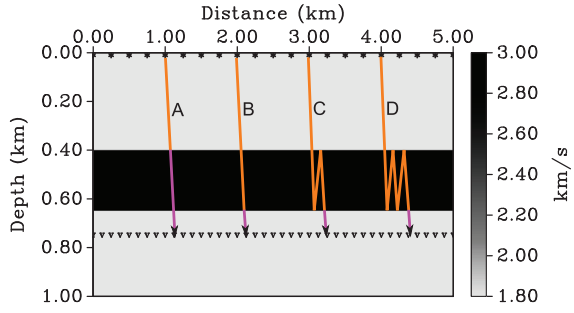

Figure 8. Interpretation of artifacts coming from the overburden reverberations in Figures 6 and 9. In this interpretation, the orange path represents the positive times and the purple path represents the negative times.

Downloaded 05/13/21 to 145.94.67.71. Redistribution subject to SEG license or copyright; see Terms of Use at http://library.seg.org/page/policies/terms
DOI:10.1190/geo2019-0208.1

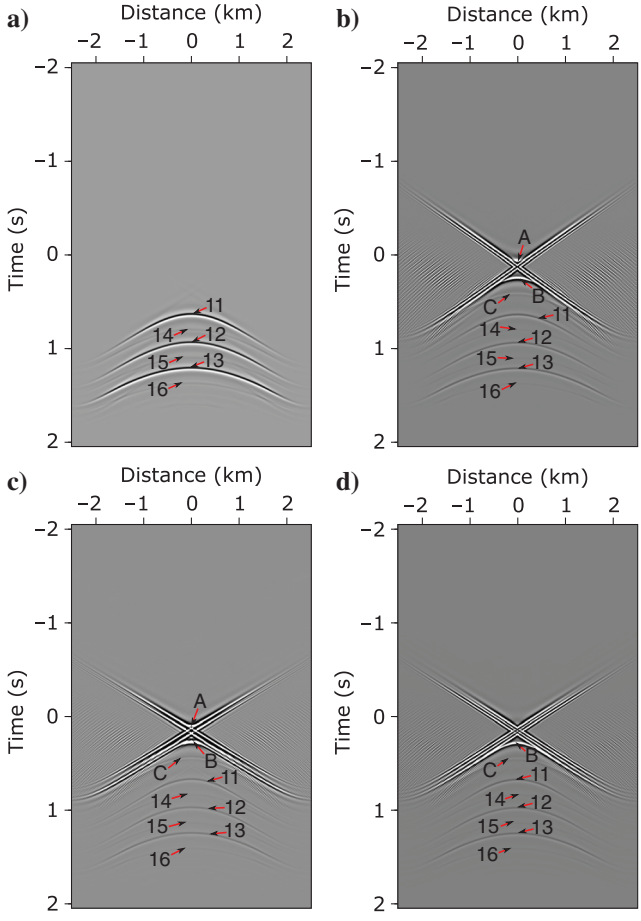

Figure 9. Upward Green's function retrieved by inversion using equation 6, in which the wave propagation is modeled in the (a) exact, (b) incorrect, (c) smoothed exact, and (d) smoothed incorrect velocity fields.

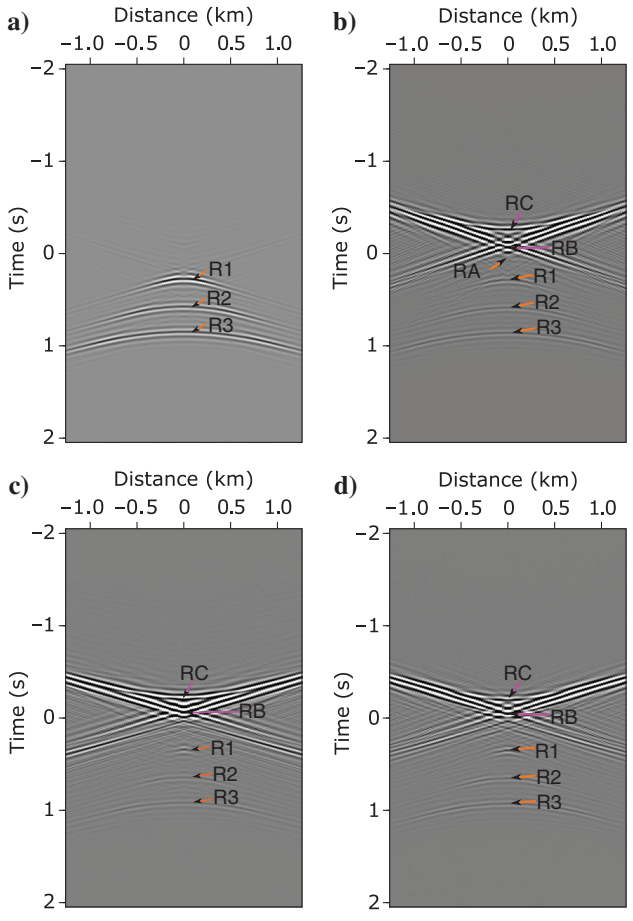

Figure 11. Results of the complete redatuming process using the set of equations 6–8, with transmitted and backscattered wavefields modeled in the (a) exact, (b) incorrect, (c) smoothed exact, and (d) smoothed incorrect velocity fields.

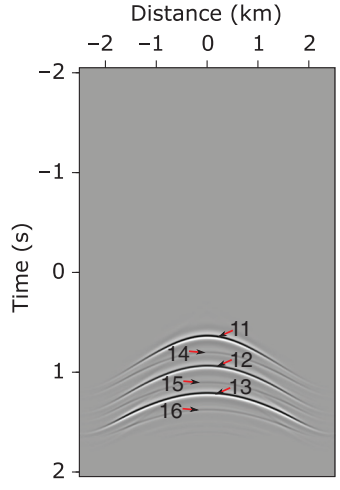

Figure 10. Upward Green's function retrieved by inversion using equation 6, with the transmitted wavefield modeled in the smoothed velocity field and the backscattered wavefield in the exact velocity model.

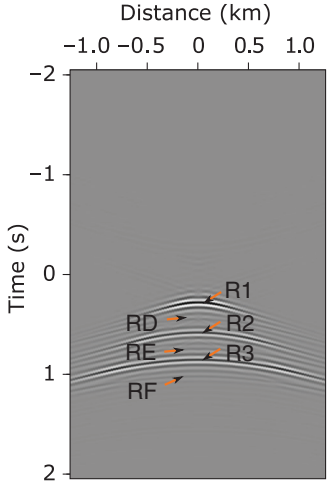

Figure 12. Results of the complete redatuming process using the set of equations 6–8, with the transmitted wavefield modeled in the smoothed velocity field and the backscattered wavefield modeled in the exact velocity model.

Downloaded 05/13/21 to 145.94.67.71. Redistribution subject to SEG license or copyright; see Terms of Use at http://library.seg.org/page/policies/terms
DOI:10.1190/geo2019-0208.1

As for the downgoing wavefield constituents, the full redatuming result is the best when the modeling of both required wavefields is done in the exact truncated velocity field (Figure 11a). The three physical events $R1$, $R2$, and $R3$ are clearly identifiable, and very few artifacts are visible, mainly those from boundary effects. The smoothed and incorrect models lead to strong artifacts (events RA, RB, and RC) that can be associated with nonphysical events (Figure 11b–11d). As expected, the wavefields in Figure 11c and 11d suffer from some mispositioning because of the velocity error in the incorrect model. When using the smoothed model for the transmitted wavefield and the exact model for the backscattered one, the desired events are still well-recovered (Figure 12) but some weak artifacts become visible (events RD, RE, and RF).

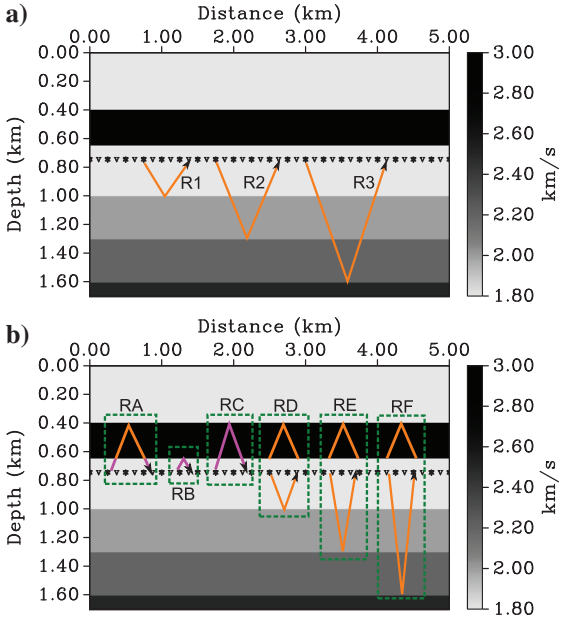

Figure 13. Raypath interpretation of the visible events in Figure 11. (a) Primary reflections from the three interfaces below the datum and (b) visible artifacts. Here, the orange path represents the positive and the purple path represents the negative traveltimes.

Figure 13 depicts the raypath interpretation of the redatumed events. Labels $R1$, $R2$, and $R3$ (Figure 13a) denote physical events corresponding to the primary reflections from the three interfaces below the datum. These events are present in all four parts of Figure 11. When the modeling is done in the exact model, they are recovered without artifacts except for boundary effects (Figure 11a). Labels RB and RC (Figure 13b) are physical events that correspond to primary reflections at the overburden reflectors from below, recorded at the position of the datum. These events appear at negative times in the records. They are visible in all parts of Figure 11, but their amplitudes are much stronger when smoothed models are used for both wavefield simulations (Figure 11b and 11c). Finally, labels RA, RD, RE, and RF denote nonphysical events (Figure 13b). Label RA is an event that combines positive and negative traveltimes. It is clearly visible only in Figure 11b, but it is hidden behind the strong artifacts in Figure 11c. Events RD, RE, and RF combine propagation paths in the overburden and below the datum in a nonphysical way (Figure 13b). They become visible when using the smoothed model for the transmitted wavefield and the exact model for the backscattered one (Figure 12).

For more details, we compare the central traces of these redatuming responses to the corresponding modeled trace at the datum. In Figure 14a, we note that, when the modeling is done in the exact truncated model, the three principal events in the causal part retrieved by inversion fit the modeled events, regarding the traveltimes and amplitudes. As expected, the velocity error in the incorrect model leads to a displacement of the events (Figure 14b). Note that the relative amplitudes are also affected by the velocity error. The smoothed velocity models lead to very similar behavior of the events (Figure 14c and 14d) as the corresponding nonsmoothed ones, except for additional artifacts.

Finally, Figure 15 shows the same comparison for the data obtained with the transmitted wavefield modeled in the smoothed velocity field and the backscattered data in the exact velocity field. We note that the resulting central trace is very similar to the one obtained using the exact velocity field for both modeling steps, preserving the quality of the kinematics and dynamics. This confirms that the sensitivity of the redatuming method studied here comes from the backscattered and not from the transmitted wavefield.

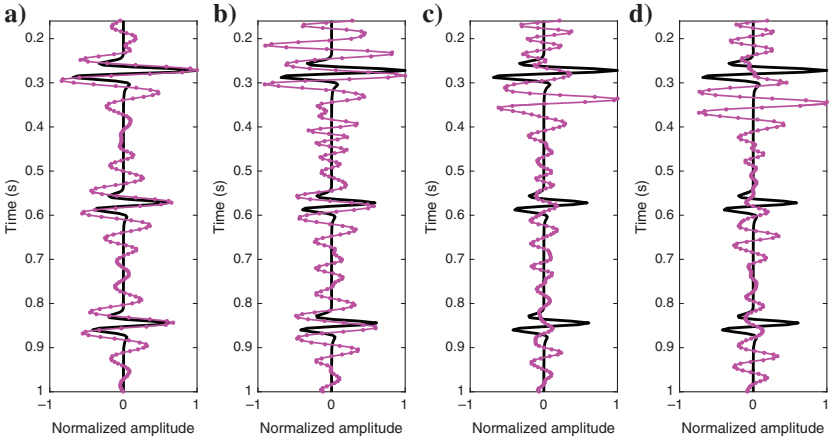

Figure 14. Central traces of the redatuming responses corresponding to the causal parts in Figure 11 (the purple line), compared with the central trace of the exact data modeled at the datum (the black line). As previously, the transmitted and backscattered wavefields are modeled in the (a) exact, (b) incorrect, (c) smoothed exact, and (d) smoothed incorrect velocity fields.

DISCUSSION

We present a new interferometric procedure entirely based on deconvolution. For the redatuming of the receivers, it gives a new interpretation to two expressions previously derived by van der Neut et al. (2015a) in the context of Marchenko imaging. They are used to estimate the up- and downgoing constituents of the Green's funtions for sources at the surface and receivers at the datum. These Green's function constituents are then the input to the conventional version of deconvolution-based interferometric redatuming of Wapenaar et al. (2011) to retrieve the redatumed wavefield for sources and receivers at the datum level.

Downloaded 05/13/21 to 145.94.67.71. Redistribution subject to SEG license or copyright; see Terms of Use at http://library.seg.org/page/policies/terms
DOI:10.1190/geo2019-0208.1

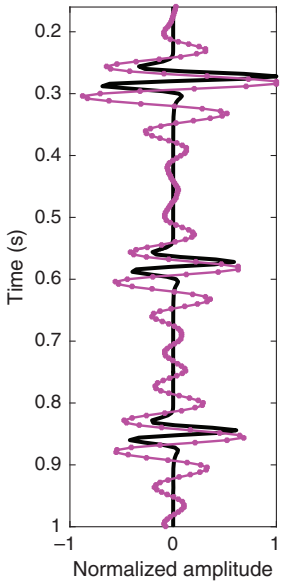

Figure 15. Central trace of the redatuming response corresponding to the causal part in Figure 12 (the purple line), compared with the central trace of the exact data modeled at the datum (the black line), with the transmitted wavefield modeled in the smoothed velocity field and the backscattered wavefield modeled in the exact velocity model.

Although the procedure relies on wavefield modeling, it does not need a full underground velocity model. It relies on a truncated model, carrying only information about the velocity field in between the acquisition surface and the datum. Outside this region, the truncated model is assumed to be homogeneous. In this truncated model, two wavefields must be simulated for sources at their original positions at the acquisition surface. These wavefields are the transmitted wavefield at the datum and the backscattered wavefield at the acquisition surface. Note that the latter is nonzero only in the case of an inhomogeneous medium between the acquisition and datum levels.

Our numerical experiments demonstrate that the procedure is capable of producing a highly accurate redatumed wavefield. Moreover, they confirm the observations of Wapenaar et al. (2011) that deconvolution-based interferometric redatuming is advantageous over a correlation-based procedure because the former automatically includes a compensation for the properties of the source wavelet, does not need the assumption of a lossless medium, and can also provide a correct treatment of internal multiples. In correlation-based procedures, internal multiples in the overburden can lead to crosstalk between uncorrelated events, generating nonphysical events in the output data (Barrera et al., 2017), even if the overburden model is perfect. In our present purely deconvolution-based procedure, such nonphysical events are reduced to a minimum. However, the use of an imperfect velocity model can also introduce nonphysical events.

The underlying wavefield modeling imposes some requirements on the quality of the truncated velocity model. Particularly, the simulation of the backscattered wavefield at the datum-overburden inhomogeneities requires a rather accurate model. When we use a smoothed truncated velocity model, no internal multiples in the overburden are modeled. As a consequence, the inverted downgoing wavefield for receivers at the datum level contain only direct waves. The corresponding upgoing wavefield still recovers all primary reflections from the medium below the datum, but it contains some high-amplitude artifacts. These artifacts are then carried over to the final redatumed data. However, because these artifacts are located at negative and small positive traveltimes, it might be possible to reduce their influence by simple muting. Our tests using a perturbed velocity model result in strong kinematic and dynamic errors, indicating that velocity errors should be kept to a minimum for the method to work reliably.

Because of the described characteristics, we think that the procedure discussed in this work will be of interest to redatum data to deeper levels if the near-surface structure is well-resolved, for example, after full-waveform inversion, which is well-known to provide high-resolution velocity models at shallow levels.

CONCLUSION

We have presented a deconvolution-based interferometric procedure to achieve the first step of full data redatuming, i.e., the determination of the downward- and upward-propagating Green's function for sources at the earth's surface and receivers at a datum in depth. Two relationships, derived from the convolution and correlation-based one-way reciprocity theorems, allow us to recover these Green's function constituents by wavefield deconvolution. The inputs to this deconvolution are the transmitted and backscattered wavefields, simulated in a truncated overburden model. The downward and upward Green's function retrieved by this procedure can then be used in conventional deconvolution-based interferometric redatuming to retrieve the reflected wavefield for sources and receivers at the datum.

As demonstrated in a simple synthetic-data example, the resulting data can be recovered almost artifact free if the overburden model is known. As a major advantage, we stress that there is no influence of anticausal events and no causal interactions with the overburden in the final responses. These types of events, which are common in purely correlation-based redatuming procedures, do not occur in the inverse wavefield extrapolation in the first and second steps of the redatuming process. However, when using a smoothed model for the wavefield simulations, some nonphysical artifacts are also present in the data redatumed with the present technique because internal multiples are no longer treated correctly. These effects can be significantly reduced if at least the backscattered wavefield is modeled in a nonsmoothed truncated velocity field. However, a sufficiently accurate overburden velocity model is required to avoid incorrect redatuming results.

ACKNOWLEDGMENTS

We are grateful to J. van der Neut for inspiring this scientific work and encouraging the first author to write about it and to K. Wapenaar for the important suggestions and comments. We thank the Brazilian agencies CNPq and FINEP, as well as Petrobras and the sponsors of the Wave Inversion Technology Consortium for their support.

DATA AND MATERIALS AVAILABILITY

Data associated with this research are available and can be obtained by contacting the corresponding author.

Downloaded 05/13/21 to 145.94.67.71. Redistribution subject to SEG license or copyright; see Terms of Use at http://library.seg.org/page/policies/terms
DOI:10.1190/geo2019-0208.1

APPENDIX A

ONE-WAY RECIPROCITY THEOREMS

Here, we revisit the derivation of the one-way reciprocity theorems of convolution and correlation type. These theorems form the basis of the new interferometric redatuming procedure based on deconvolution and inverse wave propagation proposed in this work.

Reciprocity theorems of convolution and correlation type

Following Wapenaar et al. (2010a, 2010c, 2011), we consider two states, A and B, in the Helmholtz equation to derive the reciprocity theorem of the convolution type. We assume both states to have the same properties, i.e., $\rho^A(x) = \rho^B(x) = \rho(x)$ and $c^A(x) = c^B(x) = c(x)$. Moreover, we assume that the wavefields in both states have causal sources inside volume V. Because the states differ only in the source positions, the corresponding wavefields $\hat{p}^A(x,\omega) = \hat{p}^A$ and $\hat{p}^B(x,\omega) = \hat{p}^B$ must satisfy

$$\rho(x)\nabla\cdot\left[\frac{1}{\rho(x)}\nabla\hat{p}^A\right]+\frac{\omega^2}{c^2(x)}\hat{p}^A=-\hat{F}^A, \tag{A-1}$$

$$\rho(x)\nabla\cdot\left[\frac{1}{\rho(x)}\nabla\hat{p}^B\right]+\frac{\omega^2}{c^2(x)}\hat{p}^B=-\hat{F}^B. \tag{A-2}$$

Note that equations A-1 and A-2 show that the difference between state A and state B is in the source distribution and the wavefield, while the rest of the properties remain the same. After multiplication of equation A-1 by $\hat{p}^B$ and equation A-2 by $\hat{p}^A$, their difference yields

$$\begin{aligned}\rho(x)\hat{p}^B\nabla\cdot\left[\frac{1}{\rho(x)}\nabla\hat{p}^A\right]-\rho(x)\hat{p}^A\nabla\cdot\left[\frac{1}{\rho(x)}\nabla\hat{p}^B\right]\\ =-\hat{p}^B\hat{F}^A+\hat{p}^A\hat{F}^B.\end{aligned} \tag{A-3}$$

Dividing equation A-3 by $\rho(x)$, adding and subtracting a term $\nabla\hat{p}^A\nabla\hat{p}^B$ on the left side, and manipulating and reorganizing the terms, we obtain

$$\nabla\cdot\left[\frac{1}{\rho(x)}(\hat{p}^B\nabla\hat{p}^A-\hat{p}^A\nabla\hat{p}^B)\right]=\frac{1}{\rho(x)}(\hat{p}^A\hat{F}^B-\hat{p}^B\hat{F}^A). \tag{A-4}$$

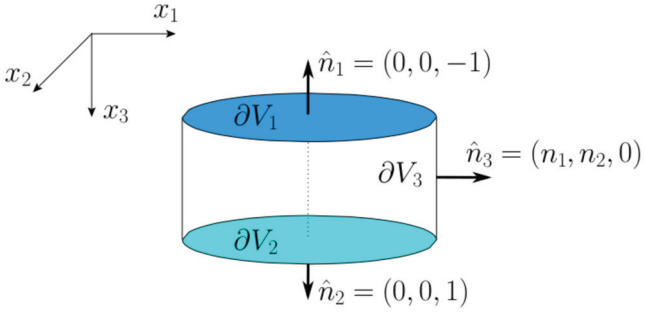

Figure A-1. Cylinder surface decomposed into three surfaces ∂V_1, ∂V_2, and ∂V_3.

After integration over an arbitrary volume V, equation A-4 has an appropriate form to apply Gauss's theorem (equation 5). The result is the reciprocity theorem of convolution type, which we can represent as

$$\begin{aligned}&\oiint_{\partial V}\frac{1}{\rho(x)}(\hat{p}^B\nabla\hat{p}^A-\hat{p}^A\nabla\hat{p}^B)\cdot\hat{n}dS\\ &=\iiint_V\frac{1}{\rho(x)}(\hat{p}^A\hat{F}^B-\hat{p}^B\hat{F}^A)dV.\end{aligned} \tag{A-5}$$

A completely analogous analysis can be carried out starting at the complex conjugate of equation A-1 together with equation A-2. Replacing the wavefield $\hat{p}^A$ and the source term $\hat{F}^A$ in the above derivation by their complex conjugates $\hat{p}^{A*}$ and $\hat{F}^{A*}$, where the superscript * denotes the complex conjugate, we correspondingly arrive at

$$\begin{aligned}&\oiint_{\partial V}\frac{1}{\rho(x)}(\hat{p}^B\nabla\hat{p}^{A*}-\hat{p}^{A*}\nabla\hat{p}^B)\cdot\hat{n}dS\\ &=\iiint_V\frac{1}{\rho(x)}(\hat{p}^{A*}\hat{F}^B-\hat{p}^B\hat{F}^{A*})dV.\end{aligned} \tag{A-6}$$

This is the reciprocity theorem of correlation type.

Using the Sommerfeld radiation condition (Bleistein et al., 2001) and the antiradiation condition (Wapenaar, 2006), it is possible to demonstrate that the left-side integrals in equations A-5 and A-6 tend to zero when the radius of the closed surface tends to infinity. However, the volume integrals on the right sides have only nonzero contributions from those parts of volume V where the source functions $\hat{F}^A$ and $\hat{F}^B$ are nonzero. Thus, their values do not change when extending volume V over regions without sources. Therefore, we can conclude that the surface integrals in equations A-5 and A-6 must be identically zero for any shape of surface ∂V as long as it includes all sources of states A and B. Of course, they are also zero if all sources of states A and B are outside V because then the volume integrals vanish.

Surface decomposition of the reciprocity theorems

In this section, we analyze the closed-surface integrals in the reciprocity theorems of convolution and correlation type (equations A-5 and A-6). Because volume V is arbitrary in these equations, it can be chosen as a cylinder. Then, the surface ∂V in equations A-5 and A-6 can be decomposed into three parts ∂V_1 (the top), ∂V_2 (the bottom), and ∂V_3 (the side of the cylinder) with the unit vectors $\hat{n}_1 = (0,0,-1)$, $\hat{n}_2 = (0,0,1)$, and $\hat{n}_3 = (n_1, n_2, 0)$, respectively (Figure A-1).

By this choice, the closed-surface integral in equation A-5 can be recast into the form

$$\begin{aligned}&\iint_{\partial V_1}\frac{1}{\rho(x)}(\hat{p}^B\nabla\hat{p}^A-\hat{p}^A\nabla\hat{p}^B)\cdot\hat{n}_1dx_1dx_2\\ &+\iint_{\partial V_2}\frac{1}{\rho(x)}(\hat{p}^B\nabla\hat{p}^A-\hat{p}^A\nabla\hat{p}^B)\cdot\hat{n}_2dx_1dx_2\\ &+\iint_{\partial V_3}\frac{1}{\rho(x)}(\hat{p}^B\nabla\hat{p}^A-\hat{p}^A\nabla\hat{p}^B)\cdot\hat{n}_3dx_1dx_2=0.\end{aligned} \tag{A-7}$$

The Sommerfeld radiation conditions require that the integral over surface ∂V_3 tends to zero when the cylinder radius is extended to

Downloaded 05/13/21 to 145.94.67.71. Redistribution subject to SEG license or copyright; see Terms of Use at http://library.seg.org/page/policies/terms
DOI:10.1190/geo2019-0208.1

infinity. Thus, we conclude that the integrals over the remaining two surfaces must satisfy

$$\iint_{S_1} \frac{1}{\rho(x)} (\hat{p}^B \nabla \hat{p}^A - \hat{p}^A \nabla \hat{p}^B) \cdot \hat{n}_1 dx_1 dx_2 = -\iint_{S_2} \frac{1}{\rho(x)} (\hat{p}^B \nabla \hat{p}^A - \hat{p}^A \nabla \hat{p}^B) \cdot \hat{n}_2 dx_1 dx_2, \quad \text{(A-8)}$$

where S_1 and S_2 denote the complete horizontal planes at two different depth levels, e.g., the acquisition level $x_3 = x_{30}$ and the datum level $x_3 = x_{3d}$, respectively. To derive equation A-8, no assumptions regarding the nature of the medium inside and outside the surface ∂V are necessary. In other words, this equation is valid for general inhomogeneous media, as long as the sources are completely inside or completely outside volume V and the medium properties in both states are the same inside the volume, i.e., between the two horizontal planes S_1 and S_2.

For the reciprocity theorem of correlation type, the analogous procedure provides

$$\iint_{\partial V_1} \frac{1}{\rho(x)} (\hat{p}^B \nabla \hat{p}^{A*} - \hat{p}^{A*} \nabla \hat{p}^B) \cdot \hat{n}_1 dx_1 dx_2 + \iint_{\partial V_2} \frac{1}{\rho(x)} (\hat{p}^B \nabla \hat{p}^{A*} - \hat{p}^{A*} \nabla \hat{p}^B) \cdot \hat{n}_2 dx_1 dx_2 + \iint_{\partial V_3} \frac{1}{\rho(x)} (\hat{p}^B \nabla \hat{p}^{A*} - \hat{p}^{A*} \nabla \hat{p}^B) \cdot \hat{n}_3 dx_1 dx_2 = 0. \quad \text{(A-9)}$$

The form of the integral over surface ∂V_3 in equation A-9 does not allow for the application of the Sommerfeld radiation conditions. However, using the Wapenaar antiradiation conditions (Wapenaar, 2006), we can also justify that this integral tends to zero when the cylinder radius tends to infinity. In effect, these conditions state that there should be no contributions from infinity to this integral in an inhomogeneous medium with sufficient scattering. Hence, the reciprocity theorem of correlation type can be written as

$$\iint_{S_1} \frac{1}{\rho(x)} (\hat{p}^B \nabla \hat{p}^{A*} - \hat{p}^{A*} \nabla \hat{p}^B) \cdot \hat{n}_1 dx_1 dx_2 = -\iint_{S_2} \frac{1}{\rho(x)} (\hat{p}^B \nabla \hat{p}^{A*} - \hat{p}^{A*} \nabla \hat{p}^B) \cdot \hat{n}_2 dx_1 dx_2 \quad \text{(A-10)}$$

again with S_1 and S_2 denoting the complete horizontal planes at $x_3 = x_{30}$ and $x_3 = x_{3d}$, respectively. Equation A-10 is valid for general inhomogeneous media inside and outside the surface ∂V, as long as the medium inside the cylinder is sufficiently inhomogeneous at far distances for the scattering to satisfy the Wapenaar antiradiation conditions.

One-way wavefield decomposition

To derive the one-way forms of the above reciprocity theorems, we consider the two states, A and B, in the situation depicted in Figure A-2. As previously, the surfaces S_1 and S_2 denote full horizontal planes at depth levels x_{30} and x_{3d}; i.e., they are given by $S_1 = \{(x_1, x_2, x_3) \in \mathbb{R}^3 | x_3 = x_{30}\}$ and $S_2 = \{(x_1, x_2, x_3) \in \mathbb{R}^3 | x_3 = x_{3d}\}$. States A and B have source positions x^A and x^B immediately above or below surface S_1, respectively, and the receivers are distributed over both surfaces. Note that we do not consider S_1 to be a free surface.

In accordance with Wapenaar and Berkhout (1989), the total wavefield $\hat{p}(x, \omega)$ at a point x in the medium can be decomposed in up- $(-)$ and downgoing $(+)$ constituents, i.e.,

$$\hat{p}(x, \omega) = \hat{p}_+(x, \omega) + \hat{p}_-(x, \omega). \quad \text{(A-11)}$$

The substitution of decomposition A-11 in the above reciprocity theorems allows us to derive the corresponding one-way reciprocity theorems of convolution and correlation type. These, in turn, are the basis for the retrieval of the up- and downgoing Green's functions using least-squares inversion.

At this point, we suppose that the sources are delta functions in space and time and that the velocity field is sufficiently smooth in a small region around surfaces S_1 and S_2. Under these assumptions, we can express the up- and downgoing pressure fields $\hat{p}_\pm(x, \omega; x^s)$ locally by means of ray-theoretical approximations of the form

$$\hat{p}_\pm(x, \omega; x^s) \sim A(x; x^s) \exp[\mp i\omega T(x; x^s)]. \quad \text{(A-12)}$$

Here, T is the traveltime function that satisfies the eikonal equation $\|\nabla T(x; x^s)\|^2 = 1/c^2(x)$, where c is the wave speed and $A(x; x^s)$ is the amplitude, principally determined by the geometric-spreading factor. Signs $(-)$ and $(+)$ in the exponential factor in equation A-12 refer to causal and anticausal responses in the time domain, respectively.

As a consequence of equation A-12, the derivatives of the up- and downgoing pressure fields $\hat{p}_\pm(x, \omega; x^s)$ can be represented in the high-frequency approximation as

$$\nabla \hat{p}_\pm \approx \mp i\omega \hat{p}_\pm \nabla T(x; x^s), \quad \text{(A-13)}$$

where the amplitude variation has been neglected compared to the phase variation. It is important to note that, when the wavefield is decomposed into its up- and downgoing components, the signs of the gradients of these individual wavefield components depend on the propagation direction.

One-way reciprocity theorems of convolution and correlation type

In this section, we derive the one-way reciprocity theorems of convolution and correlation type using the above wavefield decomposition. These theorems are helpful to extract detailed information

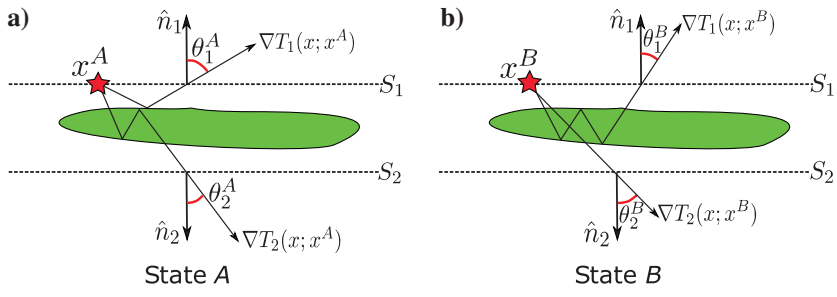

Figure A-2. Sketch of two sources at positions x^A and x^B at surface S_1 with receivers along surfaces S_1 and S_2. Also shown are the selected propagation paths to selected receivers and the angles between the propagation directions and the surface normals at these receivers.

Downloaded 05/13/21 to 145.94.67.71. Redistribution subject to SEG license or copyright; see Terms of Use at http://library.seg.org/page/policies/terms
DOI:10.1190/geo2019-0208.1

about the waves and their behavior as a function of the propagation direction.

We start our derivation at the one-way reciprocity theorem of convolution type (equation A-8). Replacing the wavefield in equation A-8 by its decomposed form according to expression A-11, we obtain

$$\begin{aligned}&\iint_{S_1}\frac{1}{\rho(x)}[(\hat{p}_+^B+\hat{p}_-^B)\nabla(\hat{p}_+^A+\hat{p}_-^A)\\&-(\hat{p}_+^A+\hat{p}_-^A)\nabla(\hat{p}_+^B+\hat{p}_-^B)]\cdot\hat{n}_1dx_1dx_2\\&=-\iint_{S_2}\frac{1}{\rho(x)}[(\hat{p}_+^B+\hat{p}_-^B)\nabla(\hat{p}_+^A+\hat{p}_-^A)\\&-(\hat{p}_+^A+\hat{p}_-^A)\nabla(\hat{p}_+^B+\hat{p}_-^B)]\cdot\hat{n}_2dx_1dx_2.\end{aligned}\tag{A-14}$$

Assuming that the medium is smooth in a small region around S_1 and S_2, the normal derivatives of the Green's function can be approximated using expression A-13. Still upon high-frequency arguments, the main contributions to the integrals in equation A-14 come from the points of stationary phase on surfaces S_1 and S_2. At those stationary points, the absolute values of the cosines of the ray angles for $\hat{p}^A$ and $\hat{p}^B$, given by $\mathbf{n}\cdot\nabla T$, are identical. As a consequence, we have, in the vicinity of the stationary points, $\hat{p}_+^B\nabla\hat{p}_+^A\approx\hat{p}_+^A\nabla\hat{p}_+^B$ and $\hat{p}_-^B\nabla\hat{p}_-^A\approx\hat{p}_-^A\nabla\hat{p}_-^B$. This implies that, to the leading order, these terms cancel each other in the integral in equation A-14. In contrast, we have, in the vicinity of the stationary points, $\hat{p}_+^B\nabla\hat{p}_-^A\approx-\hat{p}_-^A\nabla\hat{p}_+^B$ and $\hat{p}_-^B\nabla\hat{p}_+^A\approx-\hat{p}_+^A\nabla\hat{p}_-^B$, which means that these terms give equal contributions to the integral (Wapenaar and Fokkema, 2006). Hence, we can rewrite equation A-14 as

$$\begin{aligned}&\iint_{S_1}\frac{1}{\rho(x)}(\hat{p}_-^B\nabla\hat{p}_+^A-\hat{p}_-^A\nabla\hat{p}_+^B)\cdot\hat{n}_1dx_1dx_2\\&\approx-\iint_{S_2}\frac{1}{\rho(x)}(\hat{p}_-^B\nabla\hat{p}_+^A-\hat{p}_-^A\nabla\hat{p}_+^B)\cdot\hat{n}_2dx_1dx_2.\end{aligned}\tag{A-15}$$

Because surfaces S_1 and S_2 have the geometric disposition shown in Figure A-2, the versors in equation A-15 can be expressed as $\hat{n}_1=(0,0,-1)$ and $\hat{n}_2=(0,0,1)$. This allows us to express equation A-15 as

$$\begin{aligned}&\iint_{S_1}\frac{1}{\rho(x)}(\hat{p}_-^B\partial_3\hat{p}_+^A-\hat{p}_-^A\partial_3\hat{p}_+^B)dx_1dx_2\\&\approx\iint_{S_2}\frac{1}{\rho(x)}(\hat{p}_-^B\partial_3\hat{p}_+^A-\hat{p}_-^A\partial_3\hat{p}_+^B)dx_1dx_2,\end{aligned}\tag{A-16}$$

where ∂_3 denotes the derivative in the vertical direction. Equation A-16 is the one-way reciprocity theorem of convolution type.

The derivation of the one-way reciprocity theorem of correlation type follows an analogous path. For this purpose, we need the complex conjugate of expression A-11 to replace the full wavefields in equation A-10 by their decomposed expressions. We find

$$\begin{aligned}&\iint_{S_1}\frac{1}{\rho(x)}[(\hat{p}_+^B+\hat{p}_-^B)\nabla(\hat{p}_+^{A*}+\hat{p}_-^{A*})\\&-(\hat{p}_+^{A*}+\hat{p}_-^{A*})\nabla(\hat{p}_+^B+\hat{p}_-^B)]\cdot\hat{n}_1dx_1dx_2\\&=-\iint_{S_2}\frac{1}{\rho(x)}[(\hat{p}_+^B+\hat{p}_-^B)\nabla(\hat{p}_+^{A*}+\hat{p}_-^{A*})\\&-(\hat{p}_+^{A*}+\hat{p}_-^{A*})\nabla(\hat{p}_+^B+\hat{p}_-^B)]\cdot\hat{n}_2dx_1dx_2.\end{aligned}\tag{A-17}$$

Again, the principal contributions to the integrals in equation A-17 come from the stationary points on surfaces S_1 and S_2. Using the complex conjugate of equation A-13, we have, in the vicinity of the stationary points, $\hat{p}_+^B\nabla\hat{p}_+^{A*}\approx-\hat{p}_+^{A*}\nabla\hat{p}_+^B$, $\hat{p}_-^B\nabla\hat{p}_-^{A*}\approx-\hat{p}_-^{A*}\nabla\hat{p}_-^B$, $\hat{p}_+^B\nabla\hat{p}_-^{A*}\approx\hat{p}_-^{A*}\nabla\hat{p}_+^B$, and $\hat{p}_-^B\nabla\hat{p}_+^{A*}\approx\hat{p}_+^{A*}\nabla\hat{p}_-^B$ (Wapenaar and Fokkema, 2006). With these approximations, we can write equation A-17 as

$$\begin{aligned}&\iint_{S_1}\frac{1}{\rho(x)}(\hat{p}_+^B\nabla\hat{p}_+^{A*}-\hat{p}_-^{A*}\nabla\hat{p}_-^B)\cdot\hat{n}_1dx_1dx_2\\&\approx-\iint_{S_2}\frac{1}{\rho(x)}(\hat{p}_+^B\nabla\hat{p}_+^{A*}-\hat{p}_-^{A*}\nabla\hat{p}_-^B)\cdot\hat{n}_2dx_1dx_2.\end{aligned}\tag{A-18}$$

Finally, using the explicit form of the versors $\hat{n}_1=(0,0,-1)$ and $\hat{n}_2=(0,0,1)$, we can express equation A-18 as

$$\begin{aligned}&\iint_{S_1}\frac{1}{\rho(x)}(\hat{p}_+^B\partial_3\hat{p}_+^{A*}-\hat{p}_-^{A*}\partial_3\hat{p}_-^B)dx_1dx_2\\&\approx\iint_{S_2}\frac{1}{\rho(x)}(\hat{p}_+^B\partial_3\hat{p}_+^{A*}-\hat{p}_-^{A*}\partial_3\hat{p}_-^B)dx_1dx_2.\end{aligned}\tag{A-19}$$

Equation A-19 is the one-way reciprocity theorem of correlation type.

REFERENCES

Barrera, D. F., J. Schleicher, and J. van der Neut, 2017, Limitations of correlation-based redatuming methods: Journal of Geophysics and Engineering, **14**, 1582–1598, doi: 10.1088/1742-2140/aa83cb.

Bleistein, N., J. K. Cohen, and J. W. Stockwell Jr., 2001, Mathematics of multidimensional seismic imaging, migration, and inversion: Springer.

Curtis, A., 2009, Source-receiver seismic interferometry: 79th Annual International Meeting, SEG, Expanded Abstracts, 3655–3659, doi: 10.1190/1.3255626.

Curtis, A., and D. Halliday, 2010, Source-receiver wave field interferometry: Physical Review E, **81**, 046601, doi: 10.1103/PhysRevE.81.046601.

Schuster, G., 2009, Seismic interferometry: Cambridge University Press.

Slob, E., and K. Wapenaar, 2007, Electromagnetic Green's functions retrieval by crosscorrelation and cross-convolution in media with losses: Geophysical Research Letters, **4**, L05307, doi: 10.1029/2006GL029097.

van der Neut, J., 2012, Interferometric redatuming by multidimensional deconvolution: Ph.D. thesis, Delft University of Technology.

van der Neut, J., I. Vasconcelos, and K. Wapenaar, 2015a, On Green's function retrieval by iterative substitution of the coupled Marchenko equations: Geophysical Journal International, **203**, 792–813, doi: 10.1093/gji/ggv330.

van der Neut, J., and K. Wapenaar, 2016, Adaptive overburden elimination with the multidimensional Marchenko equation: Geophysics, **81**, no. 5, T265–T284, doi: 10.1190/geo2016-0024.1.

van der Neut, J., K. Wapenaar, J. Thorbecke, E. Slob, and I. Vasconcelos, 2015b, An illustration of adaptive Marchenko imaging: The Leading Edge, **34**, 818–822, doi: 10.1190/tle34070818.1.

Wapenaar, C. P. A., and A. J. Berkhout, 1989, Elastic wave field extrapolation: Redatuming of single- and multi-component seismic data: Elsevier.

Wapenaar, K., 2006, Green's function retrieval by cross-correlation in case of one-sided illumination: Geophysical Research Letters, **33**, L19304, doi: 10.1029/2006GL027747.

Wapenaar, K., D. Draganov, R. Snieder, X. Campman, and A. Verdel, 2010a, Tutorial on seismic interferometry — Part 1: Basic principles and applications: Geophysics, **75**, no. 5, 75A195–75A209, doi: 10.1190/1.3457445.

Wapenaar, K., and J. Fokkema, 2006, Green's function representations for seismic interferometry: Geophysics, **71**, no. 4, SI33–SI46, doi: 10.1190/1.2213955.

Wapenaar, K., E. Ruigrok, J. van der Neut, D. Draganov, J. Hunziker, E. Slob, and J. Thorbecke, 2010b, Green's function representation for seismic interferometry by deconvolution: 80th Annual International Meeting, SEG, Expanded Abstracts, 3972–3978, doi: 10.1190/1.3513686.

Wapenaar, K., E. Slob, and R. Snieder, 2008, Seismic and electromagnetic controlled-source interferometry in dissipative media: Geophysical Prospecting, **56**, 419–434, doi: 10.1111/j.1365-2478.2007.00686.x.

Wapenaar, K., E. Slob, R. Snieder, and A. Curtis, 2010c, Tutorial on seismic interferometry — Part 2: Underlying theory and new advances: Geophysics, **75**, no. 5, 75A211–75A227, doi: 10.1190/1.3463440.

Wapenaar, K., J. Thorbecke, J. van der Neut, F. Broggini, E. Slob, and R. Snieder, 2014, Green's function retrieval from reflection data, in absence of receiver at the virtual source position: The Journal of the Acoustical Society of America, **135**, 2847–2861, doi: 10.1121/1.4869083.

Wapenaar, K., J. van der Neut, E. Ruigrok, D. Draganov, J. Hunziker, E. Slob, J. Thorbecke, and R. Snieder, 2011, Seismic interferometry by crosscorrelation and by multidimensional deconvolution: A systematic comparison: Geophysical Journal International, **185**, 1335–1364, doi: 10.1111/j.1365-246X.2011.05007.x.

Diego Barrera received a graduate degree (2009) in geology from the Universidad Industrial de Santander (Bucaramanga, Colombia), an M.S. (2012) in geophysics from the Universidade Federal da Bahia (Salvador, Bahia, Brazil), and a Ph.D. (2017) from the Universidade Estadual de Campinas (UNICAMP) (Campinas, SP, Brazil). He had a postdoctoral position at UNICAMP until 2018. He is now working in the Supercomputing Center at SENAI CIMATEC as the leader of the Marchenko project. He has a part in the INCT-GP program as a researcher developing projects related to interferometry and Marchenko technologies.

Downloaded 05/13/21 to 145.94.67.71. Redistribution subject to SEG license or copyright; see Terms of Use at http://library.seg.org/page/policies/terms
DOI:10.1190/geo2019-0208.1